A polarization insensitive multiband absorber as a biosensor for cancer detection

BALU ASHVANTH[1,*], BACTAVATCHALAME PARTIBANE[2]
[1]*Dept. of ECE, Vel Tech Rangarajan Dr. Sagunthala R&D Institute of Science and Technology, Chennai-62, India*
[2]*Dept. of ECE, Sri Sivasubramaniya Nadar College of Engineering, Chennai-110, India*

The design and analysis of a multiband absorber that produces ten absorption peaks between 1GHz and 20GHz is discussed in this work. Perfect absorption over the operational bands is ensured by the majority of absorption bands, which exceed 90% absorptivity. The suggested absorber has a 1.6 mm thick FR4 substrate with a 10 mm by 10 mm unit cell dimension. It is made symmetric in XY plane which makes it insensitive to angle of incidence and polarization of striking electromagnetic wave. The miniaturized version of this absorber is designed to operate in THz spectrum. The sharpness of the absorption peaks brings sensing capability to the absorber and thus finds its application as a biosensor. The vast potential of this absorber in accurate sensing of different refractive index (RI) of human muscles helps in detecting various cancer cells that is confirmed with analytic results. The maximum sensitivity of this biosensor is found to be 6.43THz/RIU for detecting breast cancer. The designed absorber is fabricated with printed circuit board fabrication technology and its performance is experimentally validated that aligns with the simulation results.

(Received November 6, 2024; accepted June 4, 2025)

Keywords: Multiband absorber, Biosensor, Absorptivity, Refractive index

1. Introduction

The widespread usage of metamaterial absorbers in a wide range of applications, such as antenna, wireless communication, military, radar, aerospace, biomedical, electromagnetic compatibility, and concealing domains, has drawn attention in recent years. Because absorber-based sensors must be flexible, low-profile, affordable, and able to withstand harsh environments, designing one is a challenging undertaking. However, modern approaches have made it possible for absorber-based sensors to be affordable, versatile, and equipped with all the capabilities that are required. The research work in [1] reported a multiband absorber that operates in C, X, and Ku frequency bands. For size compactness, multilayer structure was adopted that reduces the absorber dimension to $0.034\lambda^2$. However, the absorber supports only triple bands with increased profile size because of stacking structure. The six distinct absorption peaks were realized between 2 to 18GHz in [2]. A THz absorber was designed with the same structure that detects glucose level in the blood and various cancer cells. However, the unit cell area is too huge ($0.036\lambda^2$) to be considered as perfect sensor, as size is a vital factor that affects sensitivity. The four-band absorber which achieves perfect absorption by using C4 symmetry of the unit cell is proposed in [3]. The operating bands include C, X, Ku and Ka where it seems to be polarization insensitive. However, the absorber uses conventional star shaped upper metallic layer with the unit cell area of $1.30\lambda^2$. The multilayered frequency selective surface (FSS) reported in [4] operates in dual mode that reflects signals across dual stopbands in the transmission mode and absorbs the signals in four bands in the reflection mode. The limitations is the large profile size and the usage of mechanical switching between the two modes. In the penta-band absorber of [5], the SiO_2 layer is sandwiched between two aluminum layers where the top layer has multiple U-shaped split-ring resonators (SUSRRs). The SUSRRs were packed with sealed ethanol and thus by varying the temperature of the ethanol, the absorption peaks in THz regime shift its center frequency. The absorber cum biosensor operating across THz spectrum was demonstrated in [6] that showcase the effectiveness of the reported biosensor using sensitivity. However, it operates over six bands alone and having the unit cell area of $0.011\lambda^2$. The concentric circular ring resonating structure was used as top layer in [7] that realizes absorption band at 3.71THz with the maximum Q-factor of 92.75 that resembles high selectivity. However, the conventional design was used that renders single band absorption. A near unity absorptivity was achieved by the research work [8, 9] at 4.5THz and 105GHz using asymmetric design. Although asymmetric shape leads to polarization and incidence angle sensitivity, it offers greater output variation, linearity and sensitivity along with the capability of dealing with various analyte thickness. As illustrated in [10], the over exposing of human tissue to high frequency electromagnetic waves during tumor detection can lead to tissue destruction. This could be avoided by covering the human body with absorbing surface and the multilayer structure optimization was done using the genetic algorithm. Some already implemented metamaterial absorber designs were analyzed in [11] for implementing in industrial IoT application. The various methods such as increasing electrical length, multi-resonator, multi-layers, 3D miniaturization were adopted for improving absorption and reducing absorber size. The absorber presented in [12]

has triple ITO resistive layers separated by glass materials that provides 90% absorption across the 23.2 to 33.4 GHz bandwidth. The absorptivity is maximized to 99.99% through suitably varying the resistance of ITO films. For an ultra-wideband absorber of [13], three layers of frequency selective surfaces (FSS) were used to cover the frequency range starting from 0.61GHz to 12.33GHz and they have been separated by air medium. The whole design was backed by absorbing material for the better absorption at lower frequencies. However, the usage of multiple layers increases the absorber thickness along with structural complexity. In [14], a left-handed metamaterial-based microwave absorber for Internet of Things applications was described. It was demonstrated to have dual band absorption with a peak absorption rate of more than 98% at the 2.4 and 5.1 GHz bands. The literature [15, 16] has established a technique for realizing six bands between 1THz and 5THz. In [17], a multiband THz absorber sensor for biosensing applications was described. Seven resonant bands with maximum absorption and Q factor of 99.36% and 18.59, respectively, were produced by the top layer based on the multiring structure. The tunable multiband absorber using L shaped stubs terminated with graphene at the edges was demonstrated in [18]. By open circuiting the stubs, a size miniaturization of 0.0169 λ_o^2 was realized. In [19], a six-band biosensor for identifying cancer cells and malaria was introduced. With a maximum absorption and Q factor of 99.6% and 12.5%, respectively, it was demonstrated to have polarization insensitivity and angular stability up to 50 degrees.

In this article, an absorber which has ten resonances between 2 to 20GHz is proposed. The capability of this absorber to act as a biosensor in detecting different type of cancers is demonstrated and its effectiveness is verified from the calculated sensitivity. Section 1 of this article reviews various literature which are relevant to this research work. The unit cell design is elaborated briefly in section 2 along with its transformation stages to get deep insight into the need for structural modification. Section 3 does the parametric analysis of the proposed absorber. This part of literature also verifies the absorbers angular stability and polarization insensitivity. The applicability of the absorber in medical field for the identification of cancerous human tissue is presented in section 4. The section 5 summarizes this research work with some vital points.

2. Absorber unit cell

Fig. 1 depicts the proposed absorber unit cell structure having dimension 10mm×10mm. The absorber uses FR4 dielectric material as substrate having thickness of 1.6mm with the relative permittivity of 4.4. The FR4 substrate is sandwiched between two copper layers with top and metamaterial planes. The top metamaterial consists of inner and outer square rings of lengths P_1=9.5mm, P_2=3mm, which are connected together by intermediate metallic stub lines whose dimensions are B_1=1.2mm, L_1=5mm, L_2=5mm, L_3=3.9mm, W_1=0.3mm. The second layer in the unit cell structure comprises of split square slot with intermediate rectangular slots as shown in Fig. 1. The dimensions of the interim slots are G_1=2.5mm, G_2=2.2mm, C_1=3mm, Cx=0.3mm. The area of the unit cell is 0.0069λ^2, where λ corresponds to lower operating frequency of 2.45GHz. The whole structure of unit cell is backed by a metallic reflector made of copper with an airgap between them as shown by Fig. 1 (c). To get the best performance and improved impedance matching across the majority of the operating bands, a trial was first carried out by changing the spacing of the bottom metallic conductor from $\frac{\lambda o}{4}$ to $\frac{\lambda o}{16}$. Using 2.45GHz as the lowest working band center frequency, the guided wavelength, or λo, is computed. The trail conducted indicates that the spacing should be $\frac{\lambda o}{4}$, or 3 cm.

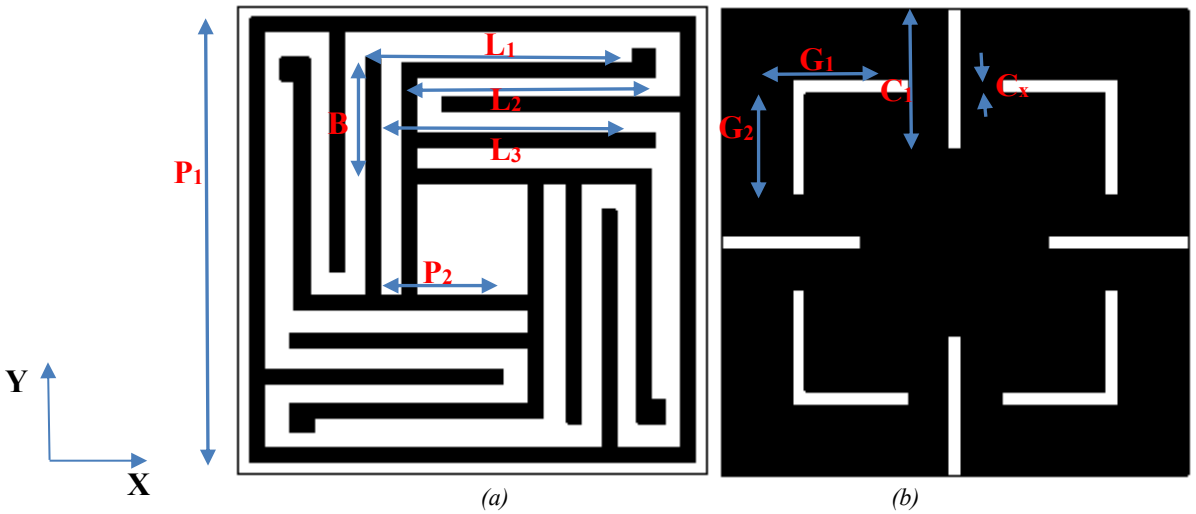

(a) (b)

(c)

Fig. 1. Absorber design a) Front view, b) Rear view, c) Side view (colour online)

Table 1. Absorber dimensions

P_1=9.5	P_2=3	B_1=1.2	L_1=5	L_2=5	L_3=3.9
W_1=0.3	G_1=2.5	G_2=2.2	C_1=3	Cx=0.3	

All dimensions are in mm

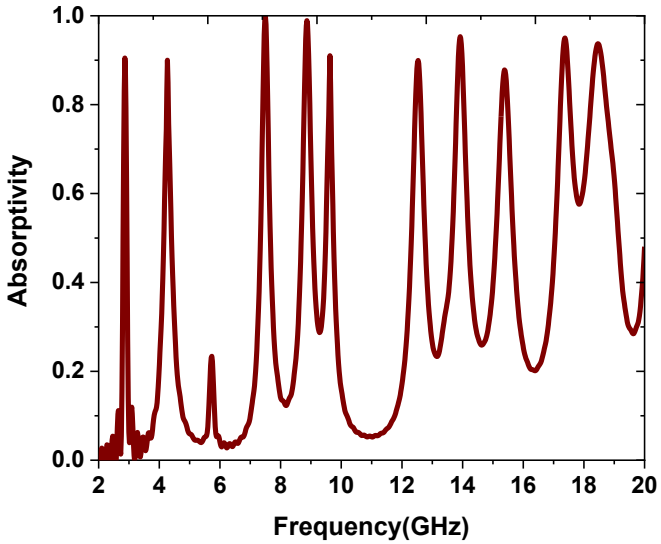

Fig. 2. Absorptivity of proposed absorber (colour online)

2.1. Evolution of absorber

Utilizing CST software for both design and simulation, the absorber is activated by designating floquet ports along the Z axis and periodic boundary conditions along the X and Y axes. Fig. 3 shows the evolution of the suggested absorber along with different design stages. Stage 1 of Fig. 3 illustrates the initial use of dual square loops, which produce resonance at 4.2GHz and 16.4GHz. Stage 2 of Fig. 3 illustrates the triple band response that results from the insertion of "L" stubs at the corners of the inner square loop. The absorption peaks of each band are located at 5.1GHz, 13.2GHz, and 19.7GHz, respectively. The third stage of absorber design involves etching slots at the corners of the intermediate plane that extend towards the center and adding a rectangular stub to each "L" stub. Tetra band resonance is created by these adjustments, with 4.2GHz, 8.1GHz, 12.9GHz, 15.3GHz, and 18GHz serving as its center frequencies. As indicated by stage 4 of Fig. 3, ten absorption bands with the corresponding center frequencies at 2.45GHz, 4.2GHz, 7.4GHz, 8.9GHz, 9.5GHz, 12.5GHz, 14GHz, 15.6GHz, 17.8GHz, and 18.8GHz are produced by attaching one additional stub to the outer square ring and by introducing a split square ring slot into the middle plane.

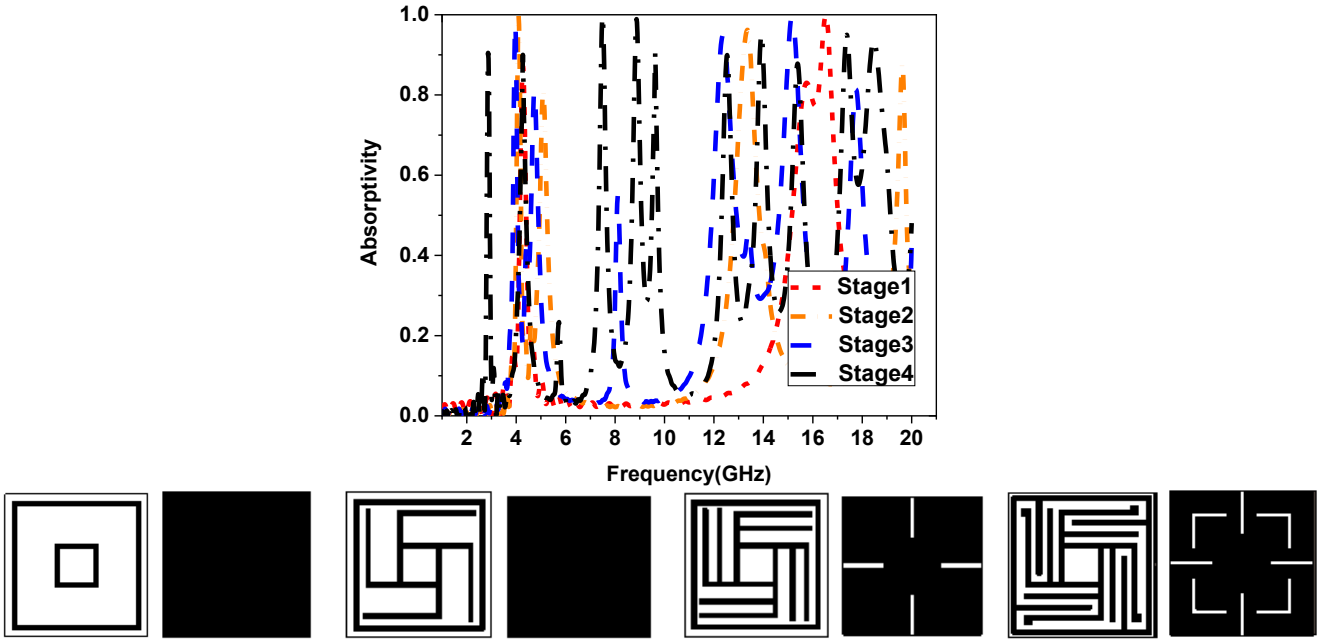

Fig. 3. Different stages of evolution of proposed absorber (colour online)

2.2. Absorber's equivalent circuit

The equivalent circuit of the absorber is illustrated in Fig. 4 and the reflection coefficient has been derived using it. Calculating the absorber's input impedance as seen from the top layer can be done by

$$Z_{in} = \frac{Z_p + jZ_s \tan(\beta h)}{Z_p \,.\, jZ_s \tan(\beta h)} \tag{1}$$

where Z_s is the characteristic impedance of the FR4 substrate, Z_p is the corresponding impedance of the top metallic layer, and β and h are the thickness and phase constant of the FR4 substrate, respectively. The following formula can be used to find the Z_p.

$$Z_p = j\omega C_1 + \frac{j(1+\omega^2 C_{12} L_{12})}{\omega L_{12}} + Z_t + \frac{j(1+\omega^2 C_{13} L_{13})}{\omega L_{13}} + R_1 \tag{2}$$

where Z_t is the top layer's internal impedance. The reflection coefficient S_{11} in decibels can be computed using the absorber's determined input impedance Z_{in} and the characteristic impedance of free space Z_0.

$$S_{11} = 20log_{10}\left(\frac{Z_{in}-Z_0}{Z_{in}+Z_0}\right) \tag{3}$$

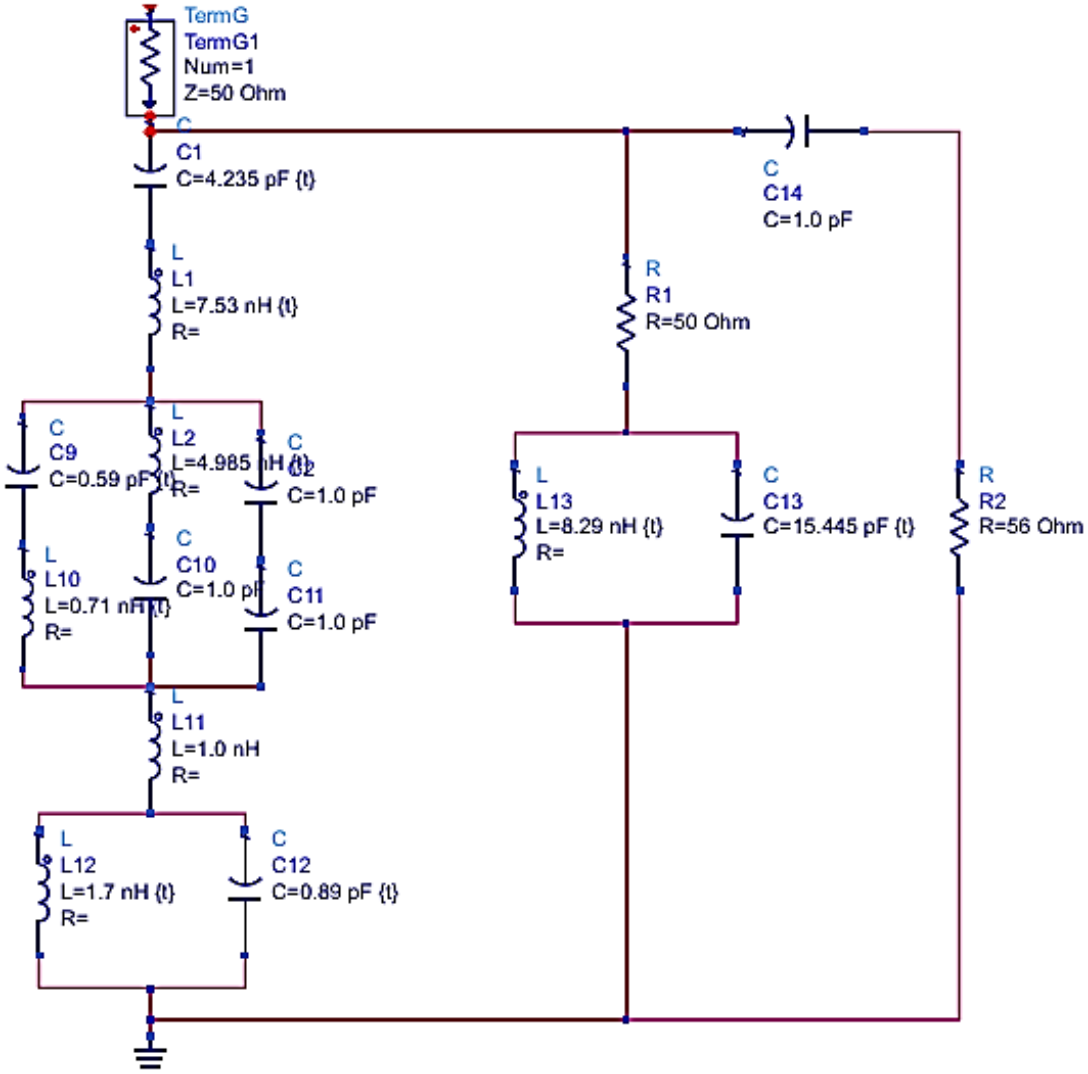

Fig. 4. Equivalent circuit for the proposed absorber (colour online)

3. Results and discussion

Fig. 5 showed the impact of top layer stub parameters on the absorption and its peak position. The absorption peak and resonance location for the 7.4GHz, 14GHz, 15.6GHz, and 17.8GHz band alter noticeably when the stub length L1 fluctuates between 4.6mm, 5mm, and 5.4mm, as shown in Fig. 5(a). In Fig. 4(b), the absorption bands centred at 8.9GHz, 9.5GHz, 14GHz, and 15.6GHz move right when the second stub length is changed from 4.6mm to 5.4mm. The peak magnitude of the latter two bands also varies. While the third stub's (L3) length variation results in changes to the absorption bands peak and position that are comparable to those of the first stub, as shown in Fig. 5(c), indicating that the responses provided by the stubs connected to the inner square ring are similar. Next, Fig. 5 (d) examines the impact of dielectric thickness on the absorption bands. The final three upper-half bands exhibit a shift to the right in terms of increasing dielectric thickness. While the higher bands shift leftwards for the exact change of the substrate thickness along with increasing bandwidth of each absorption band.

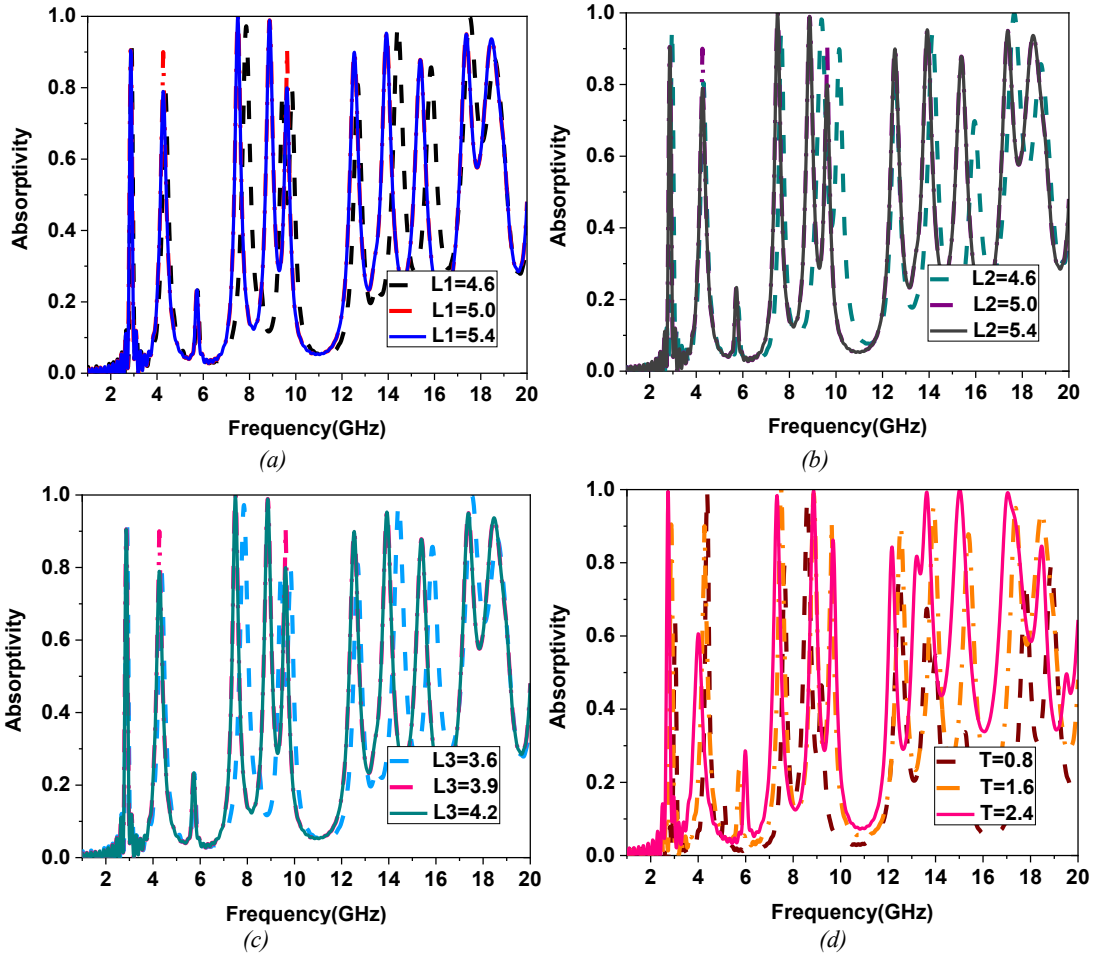

Fig. 5. Parametric analysis of proposed absorber a) L1, b) L2, c) L3, d) T (colour online)

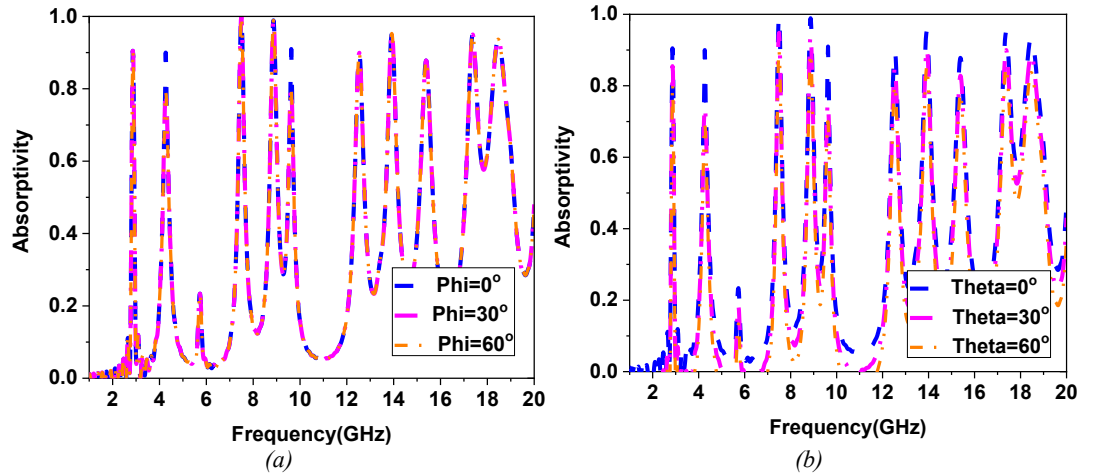

Fig. 6. Absorptivity for TE mode at different angles of (a) Phi, (b) Theta (colour online)

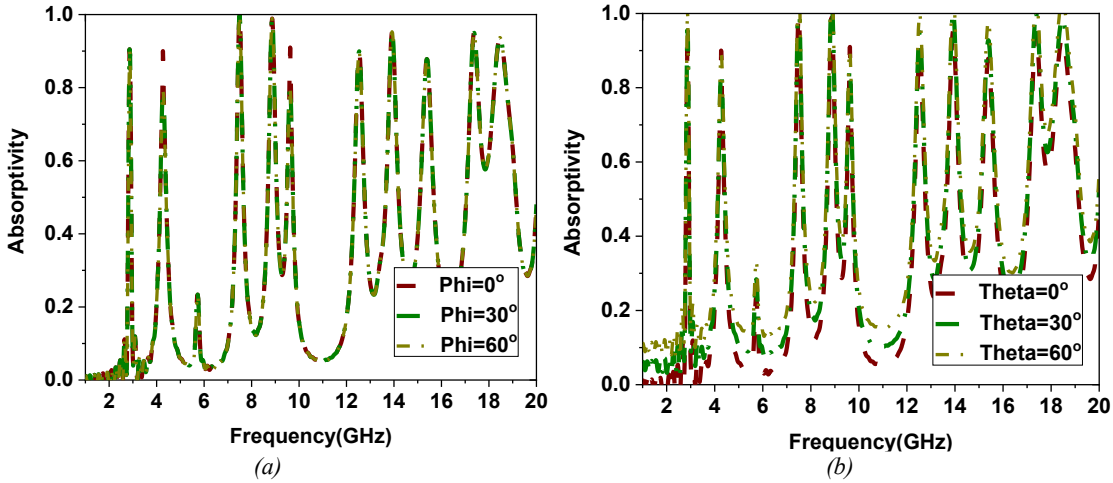

Fig. 7. Absorptivity for TM mode at different angles of (a) Phi, (b) Theta (colour online)

The absorber achieves 90%, 90%, 100%, 92%, 91%, 92%, 95%, 90%, 96%, and 95% absorption at all ten bands of 2.45GHz, 4.2GHz, 7.4GHz, 8.9GHz, 9.5GHz, 12.5GHz, 14GHz, 15.6GHz, 17.8GHz, and 18.8GHz, respectively, at normal incidence of the electromagnetic wave. The polarization angle (ϕ) is altered for both TE and TM modes in order to illustrate the suggested absorber's polarization insensitive process. To estimate the coverage angle of the absorber at TE and TM modes, the oblique incidence angle (ɵ) of the EM wave is varied while maintaining the same polarization of the incoming wave. The suggested absorber's polarization independency is made clear by varying ϕ for both the TE and TM modes of operation in Figs. 6(a) and 7(a) without causing any divergence in absorption. Figs. 6(b) and 7(b) illustrate how the absorption peak rises in each band for the TM mode and decreases in each band for the TE mode as-travel through 0° to 60°.

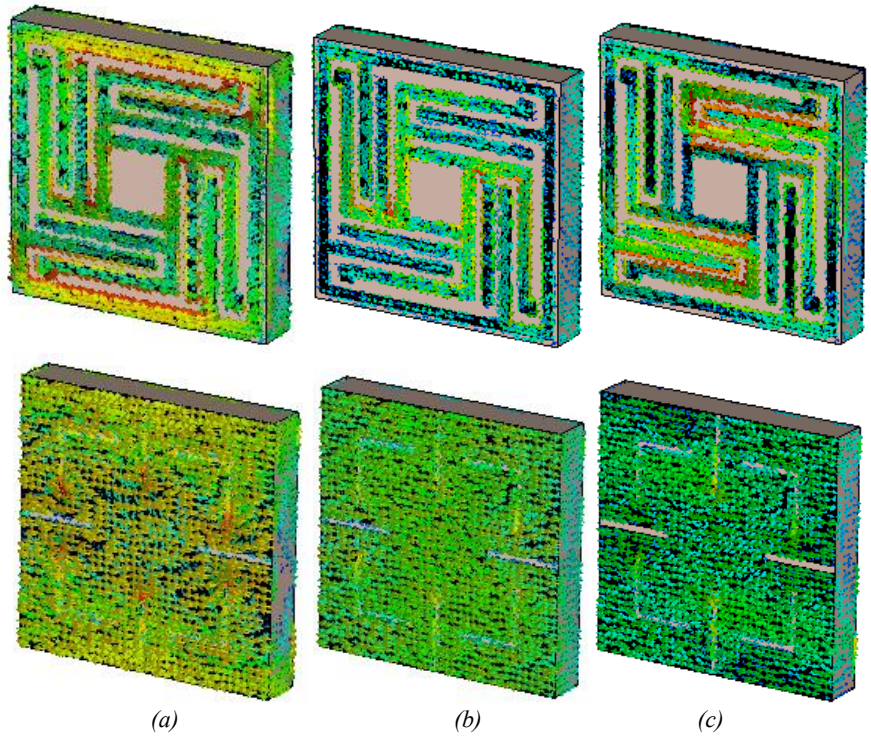

Fig. 8. Surface current distribution at the frequency of a) 2.45GHz, b) 7.4GHz, c) 12.5GHz (colour online)

Fig. 8 shows the surface current flow at three different frequencies: 2.45GHz, 7.4GHz, and 12.5GHz. Surface current analysis is crucial to understanding the behavior of the proposed absorber. According to Fig. 8(a), the current flow is greatest at 2.45GHz in the center of the bottom layer and in the outside square of the upper layer. As shown in

Figure 8(b), the surface current for the third resonant peak at 7.4GHz is found to be uniformly distributed in the bottom plane and to be at its greatest in the inner square ring of the top layer. The concentration of surface current in the upper layer is found to be at 12.5GHz at the sixth absorption peak. At the sixth absorption peak of 12.5GHz, the concentration of surface current in the top layer is found to be at its peak at the stubs connected to outer and inner square rings. While the current is sparsely distributed at the bottom surface as presented by Fig. 8 (c). The quality factor can be determined by using

$$Q = \frac{f}{FWHM} \tag{4}$$

The third band residing at the center frequency 7.4GHz is having full width half maximum (FWHM) of 0.08GHz (7.36-7.44). Its quality factor is found to be 92.5 and this ensures maximum absorption of 99.9% at this narrow band. The fabricated absorber comprises of 900 such unit cells within the area of 300×300mm^2. The measurement setup consists of horn antennas at the transmitting and receiving end isolated by a distance of 2m with a fabricated prototype at the middle as illustrated in Fig. 9 (a). The PC which is connected to the tripod of transmitting horn controls angular rotation of it. After carefully calibrating the VNA, it is indulged in the S11 measurement by connecting it with receiving horn. Comparison of simulated and measured absorptivity is depicted in Fig. 9 (b).

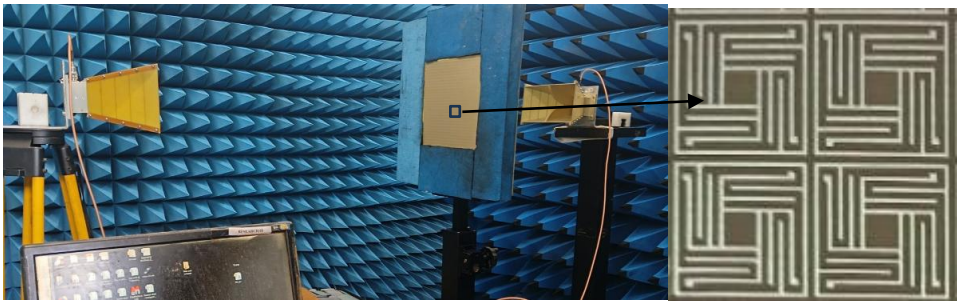

(a)

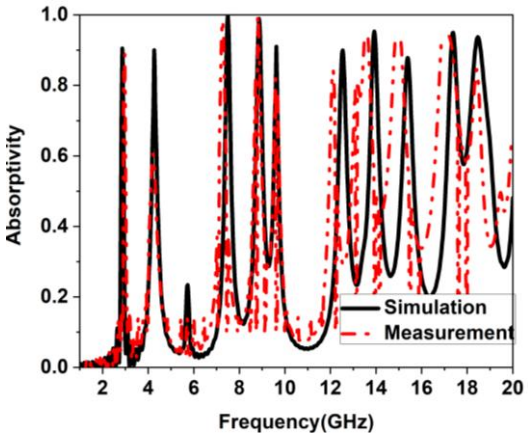

(b)

Fig. 9. Simulation and measurement result comparison (colour online)

3.1. Absorber as a biosensor

The proposed absorber unit cell has been downsized to work in THz regime for functioning as a biosensor as shown in Fig. 10 (a). The polyimide substrate of thickness 18 μm is sandwiched between two metallic layers having the respective dimensions similar to the GHz absorber as specified in Table 2.

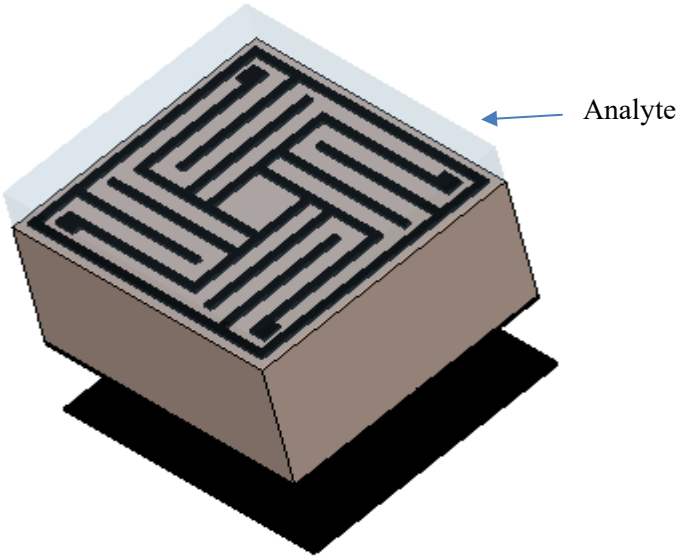

(a)

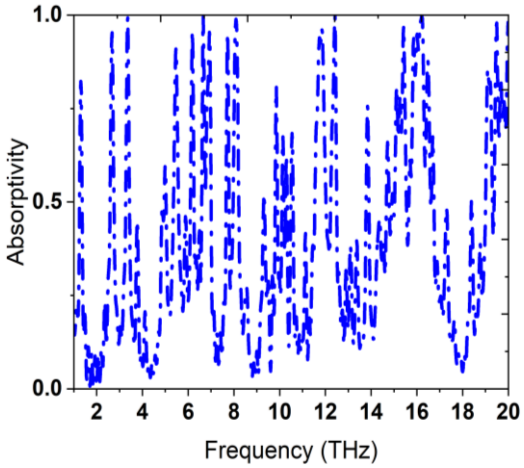

(b)

Fig. 10. Biosensor (a) Cross sectional view, (b) Absorption spectrum (colour online)

Table 2. Absorber dimensions

P_1=28	P_2=7	B_1=8	L_1=15	L_2=15	L_3=15
W_1=0.7	G_1=8	G_2=7.6	C_1=10	Cx=0.5	

All dimensions are in µm

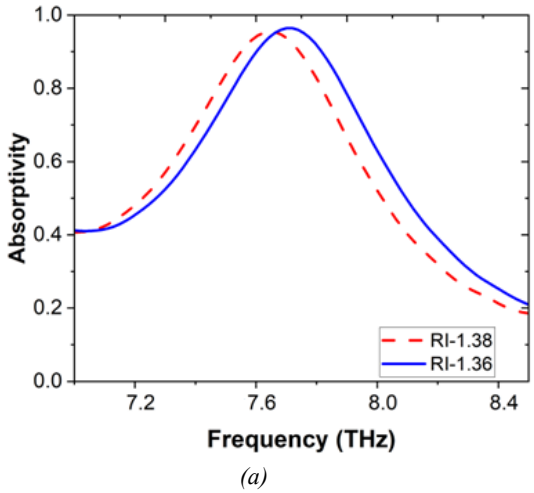

(a)

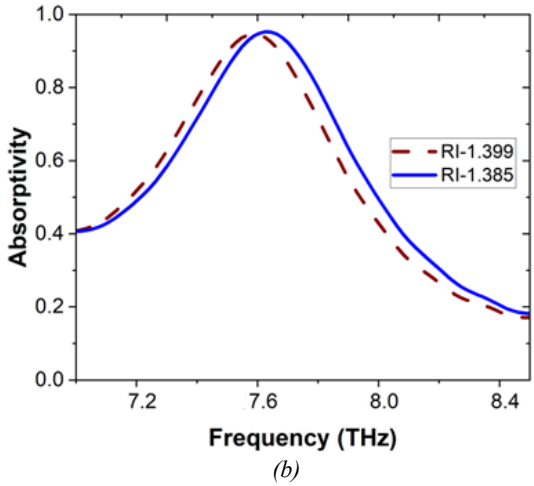

(b)

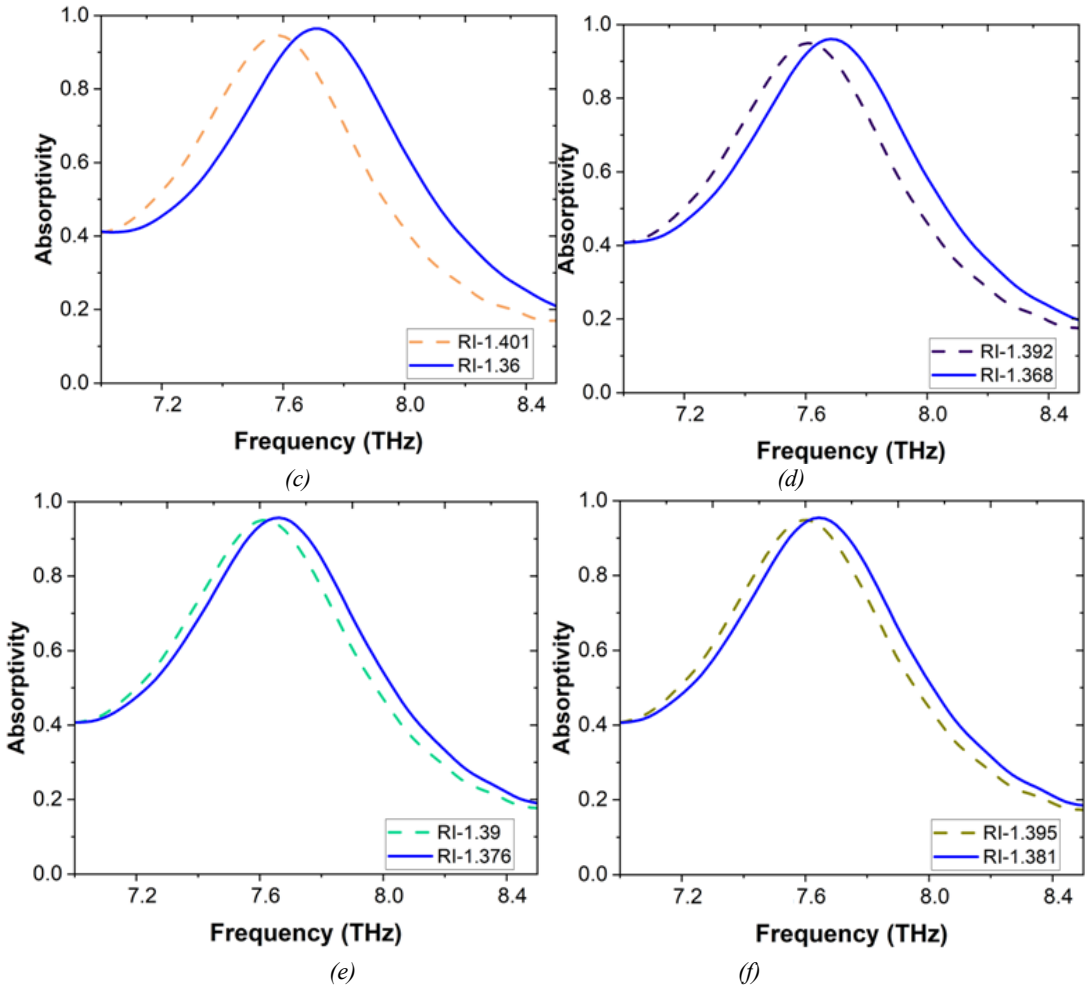

Fig. 11. Absorption peaks of biosensor for various cancer cells with respect to normal cells (a) Basal, (b) MCF-7, (c) Breast, (d) Cervical, (e) Jurkat, (f) PC-12 (colour online)

Fig. 10 (a) shows the cross-sectional view of the proposed absorber that consists of analyte at the top for sensing purpose. The proposed absorber has exceptional sensing capability due to narrow and maximized absorption peaks. This feature makes the absorber to act as a biosensor to detect various types of cancer cells. The analyte layer of fixed thickness of 5µm is included at the top of the absorber that represents the cancer muscle. The refractive index (RI) varies between normal and cancer cells. Based on the variation in the refractive index (RI) of analyte, the absorption peak shift across the spectrum of interest. The Fig. 11 illustrates the variation in the absorption peak at 7.7THz of various cancer cells on comparing with normal cells. The Fig. 11 (a) shows the basal cancer cells having RI of 1.38 peaks at 7.65THz when compared to normal cell with RI of 1.36 comprising resonance peak at 7.78THz. Fig. 11 (b) shows the comparison between MCF-7 cancer cell and the normal cell with RI of 1.399 and 1.385 with respective shift in the resonance peak from 7.62THz to 7.71THz. Fig. 11 (c) shows the change in resonance peak from 7.58THz to 7.75THz with respect to breast cancer cell and normal cell having corresponding RI of 1.401 and 1.36. Fig. 11 (d) depicts absorption peak at 7.63THz for a cervical cancer cell having RI of 1.392, while normal cell peaks at 7.72THz with RI of 1.368. The Fig. 11 (e) shows the Jurkat cancer cells having RI of 1.39 peaks at 7.63THz when compared to normal cell with RI of 1.376 comprising resonance peak at 7.69THz. Fig. 11 (f) shows the comparison between PC-12 cancer cell and the normal cell with RI of 1.395 and 1.381 with respective shift in the resonance peak from 7.61THz to 7.66THz. The sensitivity of this biosensor in detecting cancer cells can be calculated by

$$S = \frac{\Delta f_r}{\Delta n} \tag{5}$$

The sensitivity of this biosensor has been calculated for various cancer cells and it is found to be 4.3THz/RIU for basal cancer, 6.43 THz/RIU to Breast cancer, MCF-7 cancer of 4.15 THz/RIU, cervical cancer has 3.75 GHz/RIU, 4.29 THz/RIU for Jurkat cancer, PC-12 cancer detection provides 3.571 THz/RIU. Table 3 compares the proposed research work with already published works. It is inferred from the Table 1 that the proposed absorber has ten bands with the maximum absorption and Q factor of 99.9% and 92.5 respectively. This is the only absorber which has the biosensing capability at GHz frequency range and it is fabricated with low cost FR4 dielectric material.

Table 3. Comparison of proposed work with similar literature

	Unit cell Area	No. of Bands	Max. Absorption	Sensor Q-Factor	Absorber Substrate Material	Applications
[1]	$0.034\lambda_o^2$	3	98%	16.25	FR4 (2)	Absorber
[2]	$0.036\lambda_o^2$	6	98%	96	Polyimide	Biosensing
[3]	$1.30\lambda_o^2$	4	92%	19.5	FR4	Absorber
[6]	$0.011\lambda_o^2$	6	99.9%	16.1	Polyimide	Biosensing
[7]	$1.56\ \lambda_o^2$	1	99%	92.75	Polyimide	Biosensing
[17]	$0.021\ \lambda_o^2$	7	99.36%	18.59	Polyimide	Biosensing
[19]	$0.081\ \lambda_o^2$	6	99.6%	12.5	Polyimide	Biosensing
This work	$0.0069\lambda_o^2$	10	99.9%	92.5	FR4 & Polyimide	Biosensing

4. Conclusion

A multiband absorber is investigated by comparing the results of modelling and measurement. This absorber's ability to function as a biosensor to distinguish between various cancer cell types has been shown. The recommended absorber/biosensor has a maximum sensitivity of 6.43THz/RIU for detecting breast cancer cells. The simulated and experimental data show that the absorber has peak absorption of 90%, 90%, 100%, 92%, 91%, 92%, 95%, 90%, 96%, 95% at 2.45GHz, 4.2GHz, 7.4GHz, 8.9GHz, 9.5GHz, 12.5GHz, 14GHz, 15.6GHz, 17.8GHz, and 18.8GHz, respectively. By reducing the absorber's unit cell area to $0.0069\lambda^2$, the absorber's performance can be enhanced by accommodating more unit cells over a given area. With a maximum Q factor of 92.5, the proposed absorber can more accurately identify cancer cells. The suggested absorber's symmetric construction gave it broad angular stability up to 60 degrees and rendered it insensitive to polarization. Among its biosensing rivals, this absorber stands out due to the performance metrics mentioned above.

Funding statement

No fund is obtained from any financing organization.

References

[1] Punyatoya Routray, Debalina Ghosh, IEEE Letters on Electromagnetic Compatibility Practice and Applications **6**(1), 29 (2024).
[2] Deepanshu Sahu, Ekta Panwar, Ravi Panwar, IEEE Sensors Letters **7**, 12 (2023).
[3] Syed Wahab Zarin, Afzal Ahmed, Farooq A. Tahir, 2019 International Symposium on Antennas and Propagation (ISAP), 2019.
[4] Soumik Dey, Sukomal Dey, IEEE Transactions on Antennas and Propagation **71**(9), 7323 (2023).
[5] Tian Guo, Ying Zhong, Zhendong Yan, Xingting Pu, Wei Du, Fan Gao, Chaojun Tang, IEEE Sensors Journal **24**(7), 9909 (2024).
[6] Vikram Maurya, Sarthak Singhal, IEEE Sensors Journal **23**(21), 25919 (2023).
[7] Sagnik Banerjee, Purba Dutta, Amitkumar Vidyakant Jha, Bhargav Appasani, Mohammad S. Khan, IEEE Sensors Letters **6**(6), 1 (2022).
[8] Ayesha Mohanty, Om Prakash Acharya, Bhargav Appasani, S. K. Mohapatra, Mohammad S. Khan, Design of a Novel Terahertz Metamaterial Absorber for Sensing Applications. IEEE Sensors Journal **21**(20), 22688 (2021).
[9] Harbinder Singh, Amit Gupta, Rajinder Singh Kaler, Surinder Singh, Senior Member, Amoljit Singh Gill, IEEE Sensors Journal **22**(11), 10524 (2022).
[10] Tu Botao, Ye Mengqiu, Yang Zhen, Li Jinfeng, Li Guanghui, Zhang Yuejin, Chinese Journal of Electronics **32**(4), 736 (2023).
[11] Majid Amiri, Farzad Tofigh, Negin Shariati, Justin Lipman, Mehran Abolhasan, IEEE Internet of Things Journal **8**(6), 4105 (2021).
[12] Yan Li, Yunxi Wu, Da Li, Mingmin Zhu, Yang Qiu, Guoliang Yu, Erping Li, IEEE Transactions on Electromagnetic Compatibility **66**(3), 776 (2024).
[13] Liang Li, Hongwei Gao, Binchao Zhang, Junwei Wang, Cheng Jin, Microwave and Optical Technology Letters **66**(9), 1 (2024).
[14] Prem Nath Suman, IETE Journal of Research **30**(2), 1 (2024).
[15] Balu Ashvanth, B. Partibane, G. Idayachandran, Bulletin of Materials Science **44**(4), 281 (2021).
[16] Balu Ashvanth, B. Partibane, J. Optoelectron. Adv. M **25**(3-4), 112 (2023).
[17] Vikram Maurya, Sarthak Singhal, Materials Science and Engineering B **317**, 118215 (2025).
[18] Balu Ashvanth, Kanimozhi Selvi, Pramana - J. Phys. **95**, 193 (2021).
[19] Shashank Kumar Yadav, Vikram Maurya, Sarthak Singhal, IEEE Sensors Journal **24**(19), 29962 (2024).

* Corresponding author: drashvanthb@Veltech.edu.in